

Quasinormal modes of a charged loop quantum black hole

Li-Gang Zhu^{1,*}, Guoyang Fu^{1,†}, Shulan Li^{2,‡}, Dan Zhang^{1,§} and Jian-Pin Wu^{1,¶}

¹ *Center for Gravitation and Cosmology,*

College of Physical Science and Technology,

Yangzhou University, Yangzhou 225009, China

² *Department of Physics, Shanghai University, Shanghai 200444, China*

Abstract

This study presents a systematic investigation of quasinormal modes (QNMs) for probe fields—massless/massive scalar and Dirac fields—around a charged loop quantum gravity black hole (LQG-BH) characterized by the quantum parameter b_0 and the charge parameter Q . Through spectral analysis of quasinormal frequencies (QNFs), we uncover a distinct overtone outburst driven by quantum gravity effects, prominently manifested in the scalar field spectrum with the multipole quantum number $l = 0$. Both the outburst and its accompanying oscillatory patterns grow more pronounced with increasing overtone numbers. In contrast, massless scalar fields with $l > 1$ and Dirac fields exhibit delayed outburst development, with non-monotonic behavior dominating the first two overtones. Notably, increasing the charge Q universally suppresses quantum-gravity-induced features, including outbursts, non-monotonicity, and oscillations. Furthermore, we present evidence suggesting the presence of quasi-resonances in the massive scalar QNM spectrum, thereby illustrating the potential for the emergence of arbitrarily long-lived modes in this charged LQG spacetime. These findings establish a robust and universal interplay between quantum gravity effects and charge dynamics, providing new insights into the spectral properties of quantum-corrected BHs.

*zlgoupao@163.com

†FuguoyangEDU@163.com

‡shulanli.yzu@gmail.com

§danzhanglnk@163.com

¶jianpinwu@yzu.edu.cn

Contents

I. Introduction	2
II. Scalar and Dirac field over the charged ABBV black hole	6
III. Quasinormal modes	11
A. Scalar field case	13
B. Dirac field case	18
IV. Conclusions and discussions	22
Acknowledgments	23
A. Error analysis	24
B. The reduced wave equations	27
References	28

I. INTRODUCTION

Loop quantum gravity (LQG) is considered a promising contender for the theory of quantum gravity, characterized by its non-perturbative and background-independent nature [1–4]. The quantization technique developed in full LQG has been effectively employed in the symmetry reduced cosmological model, resulting in the development of loop quantum cosmology (LQC) [5–12]. An outstanding characteristic of LQC is its ability to naturally substitute the classical big bang singularity of the universe with a quantum bounce [5–19], leading to a non-singular evolution of the universe [20, 21].

The approach developed in LQC can be readily applied to the spherically symmetric Schwarzschild black hole (BH) model, thereby opening up the field of loop quantum gravity black hole (LQG-BH). For a detailed construction of the model, please refer to [22–24] and also see the reviews [25, 26]. Just as LQC can address the Big Bang singularity of the universe, the LQG-BH model can likewise resolve the interior singularity of BHs. Specifically, for the majority of LQG-BHs, the singularity is substituted with a transition surface that

connects a trapped region and an anti-trapped region.

Contrary to the LQC, which usually has a consistent treatment for various models, within the framework of the LQG-BH model, there are various models that employ different schemes to regularize and quantize the Hamiltonian constraint. In general, the LQG-BH models can be categorized into three main schemes: the μ_0 -scheme, the $\bar{\mu}$ -scheme, and the generalized μ_0 -scheme. In the μ_0 -scheme, it is assumed that the quantum regularization parameters remain constant over the whole phase space [22, 27–30]. An inherent drawback of this approach is that the final outcome is dependent on the fiducial structures introduced in the construction of the classical phase space. In addition, even in situations with low curvature, notable quantum effects may emerge, rendering these models non-physical. To eliminate the dependency on fiducial structures, the $\bar{\mu}$ -scheme is proposed, in which the quantum regularization parameters are selected as a function of the phase space variables [23, 24, 31, 32]. In particular, in this scheme with Chou’s choice [24, 32], the spacetime rapidly converges to the Schwarzschild geometry when the curvatures are low, which addresses the disadvantage of the μ_0 -scheme [33–36]. Nevertheless, the $\bar{\mu}$ -scheme is also subject to the drawback that the quantum corrections to the Schwarzschild BH horizon may be substantial, contrary to the prevailing belief that the horizon is a classical region and should not experience significant quantum corrections [23, 24]. To alleviate the aforementioned issues, several authors have recently proposed the generalized μ_0 -scheme [37–40]. In addition, the quantum collapsing model introduced in [41] offers an additional approach to mitigating these problems.

Quantum gravity effects inevitably induce subtle modifications to the effective background spacetime geometry, consequently manifesting as discernible signatures in the quasinormal mode (QNM) spectra. Particularly, a remarkable advancement has been the establishment of a connection between overtones and near-horizon geometry, first reported in Ref. [42]. This study found that even a slight near-horizon deformation can result in a sudden and significant change in the overtones, a phenomenon termed the “outburst of overtones” and metaphorically described as the “sound of the event horizon”. Subsequently, numerous studies on overtones have further demonstrated and confirmed this observation [43–62]. Moreover, the studies [45–47, 55, 56] also indicate that in some effective quantum gravity model, a non-monotonic behavior of the quasinormal frequencies (QNFs) as a function of the corrected parameters is observed as the extremal BH is approached. This phenomenon manifests most prominently in the fundamental mode characterized by the lowest multipole

quantum number. As the multipole quantum number increases, the non-monotonic behavior becomes less pronounced and gradually disappears. This suggests that the influence of the multipole quantum number begins to dominate over the effects of quantum gravity [45–47, 55, 56]. However, we emphasize that for higher multipole quantum number, the non-monotonic behavior reemerges at higher overtones [45, 47, 55, 60, 61, 63, 64], albeit developing more slowly due to the dominance of the centrifugal barrier in the effective potential. Another interesting observation is that an oscillatory pattern in the overtones as a function of the corrected parameter is detected as the extremal BH is approached [45–47, 55]. Both the non-monotonic behavior in the fundamental modes and the oscillatory pattern in the overtones may be linked to the extremal BH.

Recently, a novel and intriguing uniparametric polymerisation scheme¹ has been proposed to obtain a spherically symmetric LQG-BH [66, 67]. For the sake of convenience, we will refer this novel polymerisation scheme as the Alonso-Bardaji-Brizuela-Vera (ABBV) scheme, and thus this novel LQG-BH model as the ABBV BH. Like many other LQG-BH models, the quantum gravity effects introduced in this novel ABBV BH model removes the classical singularity. A more significant advancement is that in this model of [66, 67], the modified constraint algebra exhibits closure. Thus, the system offers a reliable and clear geometric representation that remains consistent, covariant, and unambiguous, regardless of the gauge choice on the phase space². A multitude of research have investigated various aspects of this model. Solar system test constraints are discussed in [69]. The potential detection of quantum gravity effects using eccentric extreme mass-ratio inspirals (EMRIs) is explored in [70], similar work for a LQG inspired rotating black hole can be found in [71]. Gravitational lensing and optical characteristics are studied in [72–74].

The QNMs of the ABBV BH have already been devoted to exploring the possibility of probing the quantum gravity effects through GWs [46, 64, 75, 76]. The work [46] pioneered the analysis of QNM spectra for scalar and electromagnetic perturbations in this geometry using the pseudo-spectral method (PSM). Their work revealed two universal features shared by quantum-corrected and modified gravity models: (i) overtone outbursts and (ii) oscillatory mode behavior. Notably, scalar perturbations exhibited faster decay rates with

¹ The phase space regularization technique employed in LQG is also known as polymerization [65].

² More recently, the topic of BHs and covariance in effective quantum gravity has been discussed in [68]. In this work, two LQG-BH solutions with general covariance were constructed.

higher oscillation counts compared to electromagnetic counterparts, while maintaining the Schwarzschild power-law tail structure unaffected by LQG corrections in time-domain profiles. Subsequent work by Moreira et al. [75] independently confirmed these results using Leaver’s method with Nollert improvement, extending calculations to higher overtones. The author in [64] further generalized these studies by including massless/massive scalar, electromagnetic and Dirac fields. Their analysis demonstrated that the overtone behavior is governed by near-horizon geometry, while the fundamental mode is localized at the potential barrier peak. Specially, massive fields support arbitrarily long-lived modes absent in massless cases. Additionally, they derived an analytical eikonal formula for QNMs and its post-eikonal extension as a $1/l$ expansion, where l is the multipole moment. The study presented in [76] investigated gravitational perturbations through an effective framework where quantum corrections are modeled via Einstein equations coupled to an anisotropic perfect fluid. The research identified universal characteristics, such as overtone outbursts and oscillatory behavior, within these gravitational perturbations. Additionally, the authors investigated the extent of isospectrality violation in the quasi-normal mode (QNM) spectra of GWs.

Building upon their prior methodology developed in Refs. [66, 67], Alonso-Bardaji et al. [77] proposed a significant extension of the ABBV model by incorporating electric charge and a cosmological constant. This enhanced framework enables the model to describe the dynamic spacetimes and the asymptotic boundaries. Furthermore, this extension aligns seamlessly with the generalized laws of BH thermodynamics, particularly the interplay between entropy, charge, and cosmological constant in the fourth law. In a complementary study, Borges et al. [78] established two critical results: (i) The Cauchy horizon is rigorously shown to reside within the transition surface, suggesting a quantum-gravitational mechanism for stabilizing causal structures and potentially resolving the classical instability associated with Cauchy horizons; (ii) The existence of limiting quantum gravitational states with vanishing surface gravity is demonstrated, which may correspond to the final stages of black hole evaporation or the emergence of remnant states at the Planck scale.

Our study focuses on analyzing the QNMs of scalar and Dirac fields in the spacetime of charged ABBV BH³. Especially, we work out the overtone modes of the Dirac field using

³ Gravitational and electromagnetic perturbations in this charged ABBV framework present significant

PSM, which were absent in the previous work of neutral ABBV BH [64]. In our present work, we pioneer the study of the combined influence of charge and effective quantum gravitational effects on QNMs. A noteworthy finding is that while individual parameters can induce overtone outbursts, the combined effect reveals that charge suppresses such outbursts, necessitating observation at higher overtones. The structure of our paper is as follows. In Section II, we provide a brief review of the charged ABBV BH and the dynamics of the scalar field and Dirac field. Section III presents a systematic study of the properties of QNMs. Finally, conclusions and further discussions are given in Section IV.

II. SCALAR AND DIRAC FIELD OVER THE CHARGED ABBV BLACK HOLE

In this section, we firstly present a brief overview of the charged ABBV BH, originally proposed in Ref. [77]. The charged ABBV BH represents an extension of the neutral ABBV BH model detailed in Refs. [66, 67]. Subsequently, we derive the equations of motion (EOM) governing the dynamics of scalar and Dirac fields within this spacetime. Then we analyze the properties of the resulting effective potentials, highlighting their physical implications.

Following the framework established in Refs. [66, 67], the authors of Ref. [77] proposed an effective LQG-corrected Hamiltonian incorporating electric charge as follows ⁴:

$$H_{\text{eff}} = -\frac{1}{2G\gamma\sqrt{1+\gamma^2\delta_b^2}} \left[\left(\frac{\sin(\delta_b b)}{\delta_b} + \frac{\gamma^2\delta_b}{\sin(\delta_b b)} - \frac{\gamma^2\delta_b Q^2}{\sin(\delta_b b)p_c} \right) p_b + 2cp_c \cos(\delta_b b) \right]. \quad (1)$$

Here, b , p_b , c and p_c are the conjugate variables satisfying the Poisson brackets as $\{b, p_b\} = G\gamma$ and $\{c, p_c\} = 2G\gamma$. Additionally, Q is a constant associated with the charge of the BH, γ is the Immirzi parameter, and δ_b is the polymerization parameter. The classical limit is obtained by taking $\delta_b \rightarrow 0$. It is important to emphasize that as $Q \rightarrow 0$, the effective Hamiltonian presented above reduces to the neutral case [66, 67].

From the effective LQG-corrected Hamiltonian presented in Eq. (1), the dynamical equa-

technical challenges, and we defer their investigation to future work.

⁴ In this analysis, we restrict our consideration to asymptotically flat spacetimes and thus set the cosmological constant to zero, as in [78].

tions can be derived. The solution to these equations results in the static metric below⁵:

$$ds^2 = -f(r)d\tau^2 + \frac{1}{\left(1 - \frac{r_0}{m}g(r)\right)f(r)}dr^2 + r^2d\Omega^2. \quad (2)$$

The functions $f(r)$ and $g(r)$ in the above equation are defined as follows, respectively:

$$f(r) = 1 - \frac{2m}{r} + \frac{Q^2}{r^2}, \quad (3)$$

$$g(r) = \frac{\frac{2m}{r} - \frac{Q^2}{r^2}}{1 + \sqrt{1 - \frac{b_0^2 Q^2}{(b_0^2 - 1)m^2}}}, \quad (4)$$

where b_0 is defined as $b_0 \equiv \sqrt{1 + \gamma^2 \delta_b^2}$. The constant of motion m is associated with the Komar mass at spatial infinity [67, 78]. This BH geometry is asymptotically flat at infinity and its horizons are located at

$$r_h^\pm = m \left(1 \pm \sqrt{1 - \frac{Q^2}{m^2}} \right). \quad (5)$$

It is noted that the horizons of this charged ABBV BH are the same as those of the Reissner-Nordström (RN) BH.

With the introduction of LQG gravity effects, the spacetime singularity is replaced by a transition surface, also known as the bounce, which connects a BH to a white hole (WH). The bounce radius r_0 is given by [77, 78]

$$r_0 = \frac{(b_0^2 - 1)}{b_0^2} m \left(1 + \sqrt{1 - \frac{b_0^2 Q^2}{(b_0^2 - 1)m^2}} \right), \quad (6)$$

with

$$|Q| \leq m \frac{\sqrt{b_0^2 - 1}}{b_0}. \quad (7)$$

It is found that the Cauchy horizon is always hidden within the bounce radius r_0 , satisfying the inequality $r_h^- < r_0 < r_h^+$ [78].

Next, we investigate the response of the charged ABBV black hole to external perturbations generated by a scalar field Ψ and a Dirac field Υ . The dynamics of these fields are governed by the following equations:

$$\frac{1}{\sqrt{-g}} \partial_\nu (g^{\mu\nu} \sqrt{-g} \partial_\mu \Psi) - \mu^2 \Psi = 0, \quad (8)$$

$$\gamma^\alpha \left(\frac{\partial}{\partial x^\alpha} - \Gamma_\alpha \right) \Upsilon = 0, \quad (9)$$

⁵ For a detailed derivation, see Ref. [77], where the results were first derived, and Ref. [78] for subsequent developments.

where $g_{\mu\nu}$ is the background metric of the charged ABBV spacetime, μ denotes the scalar field mass, γ^α are the gamma matrices, and Γ_α represents the spin connection in the tetrad formalism [79].

Through a separation of variables in the static spherically symmetric background, both equations can be reduced to a unified Schrödinger-like wave equation:

$$\frac{\partial^2 \psi}{\partial r_*^2} + (\omega^2 - V_i) \psi = 0, \quad (10)$$

where r_* is the tortoise coordinate defined by

$$\frac{dr_*}{dr} = \left(1 - \frac{2m}{r} + \frac{Q^2}{r^2}\right)^{-1} \sqrt{\left(1 - \frac{r_0}{m}g(r)\right)^{-1}}. \quad (11)$$

The effective potentials V_i exhibit distinct structures for scalar and Dirac fields. For the scalar perturbation:

$$V_{\text{scalar}} = f(r) \left(\frac{l(l+1)}{r^2} + \mu^2 \right) + \frac{f(r) [2(m - r_0 g(r)) f'(r) - r_0 f(r) g'(r)]}{2mr}, \quad (12)$$

while for the Dirac field, the spin-dependent potentials are:

$$V_{\text{Dirac}}^\pm = f(r) \frac{k^2}{r^2} \pm \frac{k \sqrt{f(r) \left(1 - \frac{r_0}{g(r)}\right)} (-2f(r) + r f'(r))}{2r^2}. \quad (13)$$

Here, the multipole quantum numbers $l = 0, 1, 2, \dots$ for the scalar field, and $k = 1, 2, 3, \dots$ for the Dirac field. V_{Dirac}^+ and V_{Dirac}^- correspond to spin-up and spin-down fermionic modes, respectively. These potentials are interrelated via a Darboux transformation [80, 81], which allows them to be mutually transformed. For brevity, this work focuses exclusively on the V_{Dirac}^+ case.

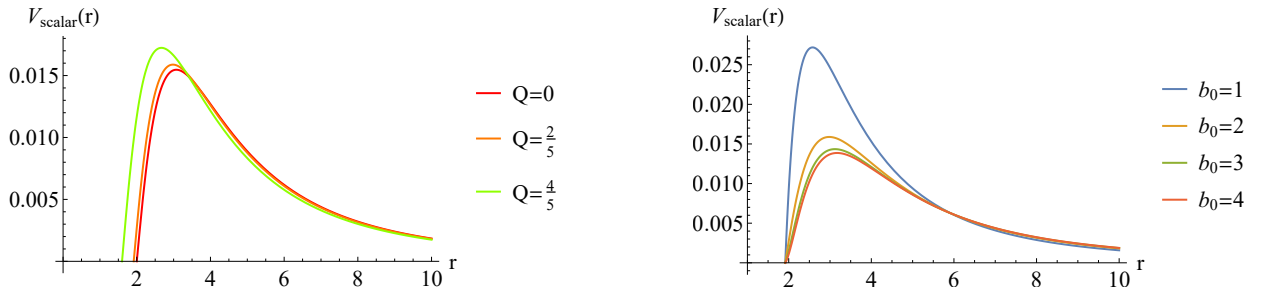


FIG. 1: The effective potential of massless scalar field as a function r with $l = 0$, while considering various values for both the quantum parameter b_0 and the charge Q . In the left panel, we fix the quantum parameter $b_0 = 2$, and then take the charge as $Q = 0, \frac{2}{5}, \frac{4}{5}$. Conversely, in the right panel, we set $Q = \frac{2}{5}$, and then the quantum parameter as $b_0 = 1, 2, 3, 4$.

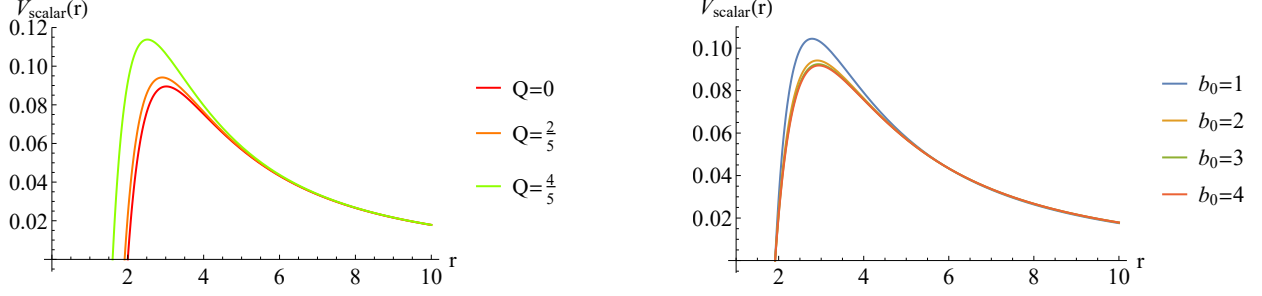


FIG. 2: The effective potential of massless scalar field as a function r with $l = 1$, while considering various values for both the quantum parameter b_0 and the charge Q . In the left panel, we fix the quantum parameter $b_0 = 2$, and then take the charge as $Q = 0, \frac{2}{5}, \frac{4}{5}$. Conversely, in the right panel, we set $Q = \frac{2}{5}$, and then take the quantum parameter as $b_0 = 1, 2, 3, 4$.

We begin by analyzing the effective potential V_{scalar} for a massless scalar field, which is structurally decomposed into two distinct components as defined in Eq.(12). The first term is the centrifugal potential, associated with the multipole quantum number l . The centrifugal potential prevents the wave from approaching the center, forming a barrier in regions farther away from it. The second term is the gravitational potential, related to the gravitational field or the geometry of spacetime, which typically introduces additional attraction or barriers, influencing the wave's decay characteristics. Notably, the quantum parameter b_0 appears only in the second term, making the effects of quantum gravity most significant when $l = 0$. As l increases, the influence of the multipole quantum number tends to overshadow the quantum gravity effects—a phenomenon observed in our previous work [46, 47, 55, 56]. Therefore, to better explore the effects of quantum gravity and charge Q , we focus primarily on the $l = 0$ case and then briefly discuss the $l = 1$ case.

Fig.1 and Fig.2 illustrate the effective potential V_{scalar} as a function of r for varying Q and b_0 in the case of $l = 0$ and $l = 1$, respectively⁶. The effective potential remains positive throughout, indicating the stability of the charged ABBV BH under scalar perturbations. Moreover, it is observed that the charge parameter Q and the quantum parameter b_0 predominantly affect the behaviors of the effective potential near the horizon. It is a significant factor in inducing the so-called overtone's outburst, as will be demonstrated below.

Before proceeding, we provide a qualitative analysis of the properties of the effective

⁶ Unless otherwise specified, we will set $m = 1$ throughout this paper.

potential V_{scalar} , focusing on its implications for the QNMs characteristics discussed in subsequent sections. We first examine the case with fixed b_0 (see the left plots in Fig.1 and Fig.2). From these plots, it is evident that the relative change for $Q = \frac{2}{5}$ or $Q = \frac{4}{5}$ (relative to $Q = 0$) is larger for $l = 1$ than for $l = 0$. This arises from the inclusion of the charge parameter in the centrifugal potential, where the increase in l results in a combined effect of l and Q , which induces such significant deviations. Next, we consider the case with the charge parameter Q fixed (see the right plots in Fig.1 and Fig.2). Compared to the case of $b_0 = 1$, the relative change with $b_0 > 1$ is more pronounced for $l = 0$ than for $l = 1$. This is because, as l increases, the influence of the multipole quantum number tends to overshadow the effects of quantum gravity.

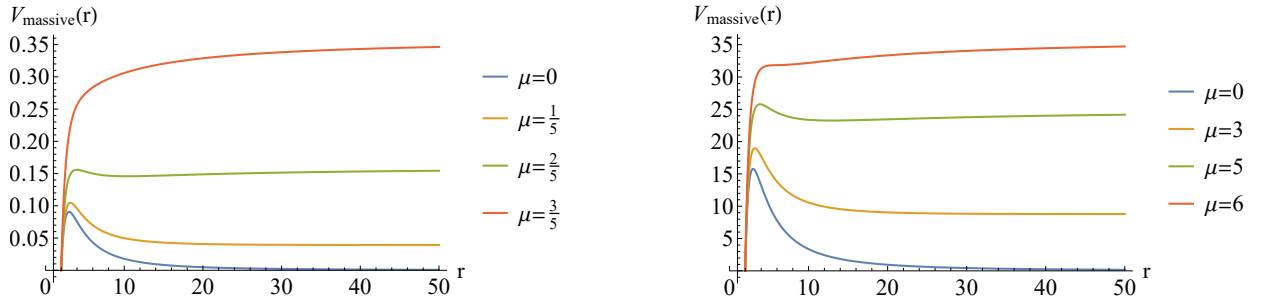


FIG. 3: The effective potential of massive scalar field as a function r with $Q = \frac{1}{5}$, $b_0 = 2$, while considering various values for mass of saclar fields μ . In the left panel, we set the $l = 1$, and then take the mass of saclar fields as $\mu = 0, \frac{1}{5}, \frac{2}{5}, \frac{3}{5}$. In the right panel, we set $l = 20$, and then the quantum parameter as $\mu = 0, 3, 5, 6$.

We now analyze the properties of the effective potential for the massive scalar field. As evident from the potential V_{scalar} (Eq.(12)), the asymptotic behavior of V_{scalar} differs significantly from the massless case: at spatial infinity ($r \rightarrow \infty$), the potential approaches a constant value μ^2 , in contrast to the vanishing behavior ($V_{\text{scalar}} \rightarrow 0$) for massless fields. This distinction is also explicitly demonstrated in Fig. 3. The inclusion of the mass term μ^2 raises the overall height of the potential, particularly in far-field regime ($r \gg 2M$), where it may form a more pronounced barrier. This affects the reflection and transmission properties of the waves, thereby altering both the oscillation frequencies and damping times of the QNMs.

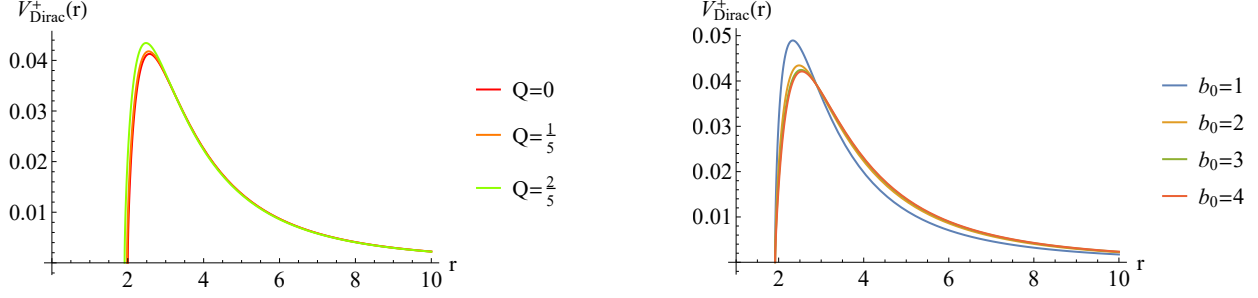


FIG. 4: The effective potential of Dirac fields as a function r with $k = 1$, while considering various values for both the quantum parameter b_0 and the charge Q . In the left panel, we fix the quantum parameter $b_0 = 2$, and then take the charge as $Q = 0, \frac{1}{5}, \frac{2}{5}$. Conversely, in the right panel, we set $Q = \frac{2}{5}$, and then take the quantum parameter as $b_0 = 1, 2, 3, 4$.

For the Dirac field, both the centrifugal and gravitational potential components exhibit explicit dependence on the multipole quantum number k . As illustrated in Fig. 4, the effective potential V_{Dirac}^+ displays a universally positive profile, indicating the stability of the charged ABBV black hole under Dirac field perturbations. While parametric tuning of the LQG-corrected parameter b_0 or the charge Q induces qualitative similarities in the potential change between Dirac and scalar fields, the amplitude of variation in V_{Dirac}^+ is systematically suppressed compared to its scalar counterpart.

III. QUASINORMAL MODES

In this section, we investigate the properties of QNMs generated by scalar and Dirac field perturbations in the context of charged ABBV BH. The QNMs are obtained by solving an eigenvalue problem under specific boundary conditions: the wave function must represent a purely outgoing wave at spatial infinity ($r_* \rightarrow +\infty$) and a purely ingoing wave at the event horizon ($r_* \rightarrow -\infty$). Mathematically, this is expressed as:

$$\psi \sim e^{\pm i\omega r_*}, \quad r_* \rightarrow \pm\infty. \quad (14)$$

These boundary conditions reflect the BH's response to a transient perturbation, capturing the dynamics after the perturbing source has dissipated [80, 82, 83].

A variety of methods have been developed to calculate QNMs, including the WKB method [84–89], the asymptotic iteration method (AIM) [90–92], the Horowitz-Hubeny method [93],

the continued fraction method (CFM) [94], and the PSM [95, 96]. In this study, we primarily utilize the PSM to calculate the QNM spectra, given its effectiveness as a robust numerical tool [45–47, 55, 56, 95–102], particularly in resolving overtone modes [46, 47, 55]. To rigorously validate the reliability of our PSM-based QNM analysis, we compare the PSM results with those obtained from the higher-order WKB method for the fundamental modes. A comprehensive discussion of this comparison is presented in Appendix A.

To determine the QNM spectra using the PSM, two key steps are essential: first, working in Eddington-Finkelstein coordinates; second, discretizing the differential equations and solve the resulting generalized eigenvalue problem. The choice of Eddington-Finkelstein coordinates simplifies the boundary condition setup. To this end, we introduce the following transformations ⁷:

$$r = \frac{r_h}{u}, \quad \text{and} \quad \psi \rightarrow e^{i\omega r_*(u)} \psi. \quad (15)$$

These transformations allow us to impose only the outgoing boundary condition at infinity. Note that, to simplify notation, we will henceforth abbreviate the outer event horizon r_h^+ as r_h . With the above considerations, the wave equation (11) is transformed into:

$$\alpha_0 \psi'' + \beta_0 \psi' + \gamma_0 \psi = 0. \quad (16)$$

The specific forms of the coefficients α_0 , β_0 , and γ_0 for both the massless scalar field and the Dirac field are detailed in Appendix B.

Next, we discretize the continuous variables using a set of Chebyshev grids and express the functions in terms of Lagrange cardinal functions. The Chebyshev grid points and the Lagrange cardinal functions are defined as follows:

$$x_i = \cos \left(\frac{i}{N} \pi \right), \quad (17)$$

$$C_j(x) = \prod_{i=0, i \neq j}^N \frac{x - x_i}{x_j - x_i}, \quad i = 0, \dots, N. \quad (18)$$

Following these operations, the wave equation is reduced to a generalized eigenvalue problem of the form:

$$(M_0 + \omega M_1) \psi = 0, \quad (19)$$

⁷ In the case of Dirac field, we use the transformations: $r = r_h/1 - u^2$, taken from [58].

where $M_i (i = 0, 1)$ represents a linear combination of the derivative matrices. The QNFs are then determined by solving this generalized eigenvalue equation.

Next, we will explore the properties of the scalar field and the Dirac field over the charged ABBV BH, respectively.

A. Scalar field case

We begin by studying the massless scalar field case with $l = 0$, where only the gravitational potential remains. Fig.5 illustrates the real part, ω_R , and the imaginary part, ω_I , of the fundamental modes as functions of the quantum parameter b_0 for various values of the charge parameter Q . When Q is fixed, an increase in b_0 leads to a monotonic decrease in ω_R and a monotonic increase in ω_I . This behavior is consistent with the uncharged case (the black line for $Q = 0$ and also see Refs.[46, 64]). These observations suggest that the LQG effect reduces the oscillation behavior but simultaneously causes a slower decay of the modes, independent of the charge parameter Q .

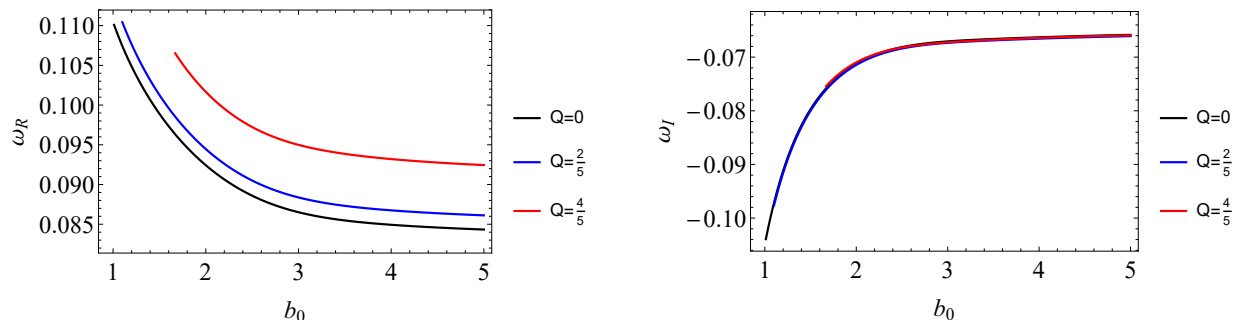


FIG. 5: For massless scalar field, QNFs of fundamental modes are presented as a function of the quantum parameter b_0 for $l = 0$, while considering various vales of the charge, specifically $Q = 0, \frac{2}{5}, \frac{4}{5}$.

In Fig.6, we fix the quantum parameter b_0 and investigate how the fundamental modes change with Q . When $b_0 \neq 1$, the real part of the frequency, ω_R , shows a monotonic increase as Q increases (left plot in Fig.6), whereas the imaginary part, ω_I , remains nearly constant across a broad range of Q (see the right plots in Fig.6). However, for large values of Q , ω_I shows a slight increase. These findings suggest that the charge Q in this model enhances the oscillatory behavior while having minimal effect on the decay of the modes.

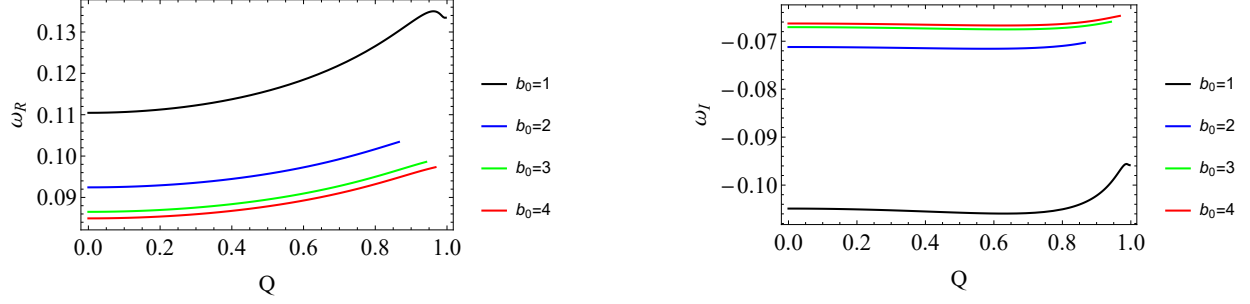


FIG. 6: For massless scalar field, QNFs of fundamental modes are presented as a function of the charge Q for $l = 0$, while considering various values of the quantum parameter, specifically $b_0 = 1, 2, 3, 4$.

Different from the previous effective quantum gravity models [45–47, 55, 56], we do not observe non-monotonic behavior of the QNFs with respect to either the quantum parameter b_0 or the charge parameter Q . However, it is worth noting that when $b_0 = 1$ corresponding to the RN scenario, both ω_R and ω_I as functions of Q display non-monotonic behavior as the extremal BH is approached, i.e., as Q tends to 1 (see the black line in Fig.6). Therefore, concerning non-monotonic behaviors, b_0 and Q play mutually inhibiting roles.

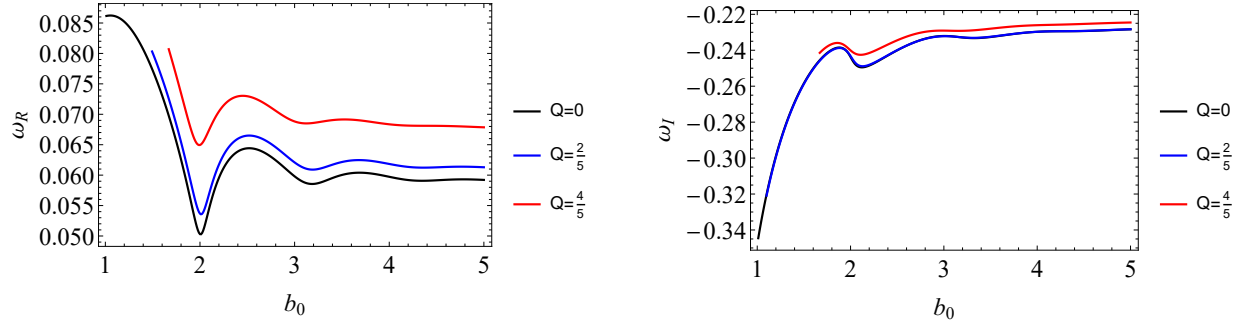


FIG. 7: For massless scalar field, QNFs of the first overtone ($n = 1$) with $l = 0$ are presented as a function of the quantum parameter b_0 for the values of the charge $Q = 0, \frac{2}{5}, \frac{4}{5}$. The left and right panels show the real and imaginary parts, respectively.

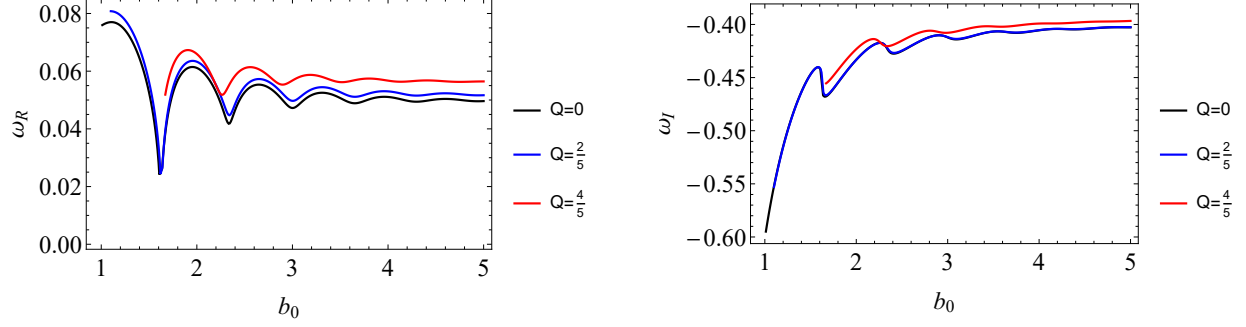


FIG. 8: For massless scalar field, QNFs of the second overtone ($n = 2$) with $l = 0$ are presented as a function of the quantum parameter b_0 for the values of the charge $Q = 0, \frac{2}{5}, \frac{4}{5}$. The left and right panels show the real and imaginary parts, respectively.

We proceed to study the properties of the overtones with $l = 0$. Fig.7 and Fig.8 show the QNFs as functions of the quantum parameter b_0 for various values of Q , corresponding to the first two overtones (Fig.7 for $n = 1$ and Fig.8 for $n = 2$, respectively). It is evident that the quantum gravity effects trigger the outburst of overtones, resulting in noticeable changes in the QNFs compared to those of Schwarzschild or RN BHs. This phenomenon has been widely observed in the modified gravity theory and effective quantum gravity models [42–60]. Following the initial outburst of overtones, we observe an oscillatory behavior. This oscillation gradually becomes weak as the quantum parameter b_0 increases. This pattern has been observed in RN-BH [103, 104] and other effective quantum gravity corrected BH [46, 47, 55] and is likely associate with the extremal effect.

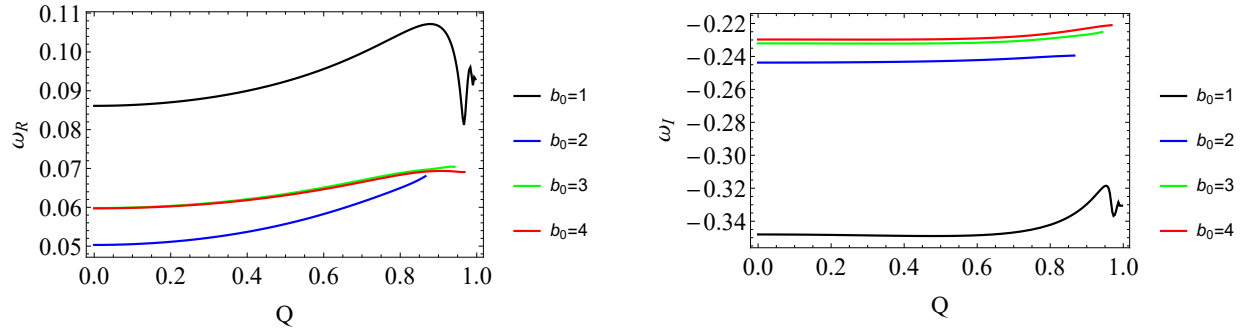


FIG. 9: For massless scalar field, QNFs of the first overtone ($n = 1$) with $l = 0$ are presented as a function of the charge Q for different quantum parameters $b_0 = 1, 2, 3, 4$. The left and right panels show the real and imaginary parts, respectively.

As expected, with increasing n , the overtone outburst becomes more pronounced, with

smaller quantum parameters capable of triggering this outburst. For fixed n , the oscillatory behavior remains consistent across different charge parameters Q . Additionally, as n increases, the oscillations become stronger. On the other hand, as Q increases, both the strength of the overtone outburst and the oscillation become weak, suggesting that the charge does not enhance either the overtone outburst or the oscillatory behavior.

We now study the behavior of the QNFs as functions of Q with a fixed b_0 (see Fig.9 and Fig.10). In the case where $b_0 = 1$, corresponding to the RN-BH, an overtone outburst with a distinct oscillatory pattern is observed (Fig.9). As the overtone number n increases, both the intensity of the overtone outburst and the prominence of the oscillations become more pronounced. Nevertheless, upon activation of the quantum parameter b_0 ($b_0 > 1$), the overtone outburst vanishes for the first overtone within the allowed range of Q (see Fig.9). For the second overtone, once the quantum parameter b_0 is activated, the overtone outburst degenerates into non-monotonic behavior (see Fig.10). In conclusion, the charge Q and the quantum parameter b_0 appear to exert mutually suppressive effects on the overtone outburst. The analogous effect on non-monotonic behaviors has also been noted in the preceding subsection.

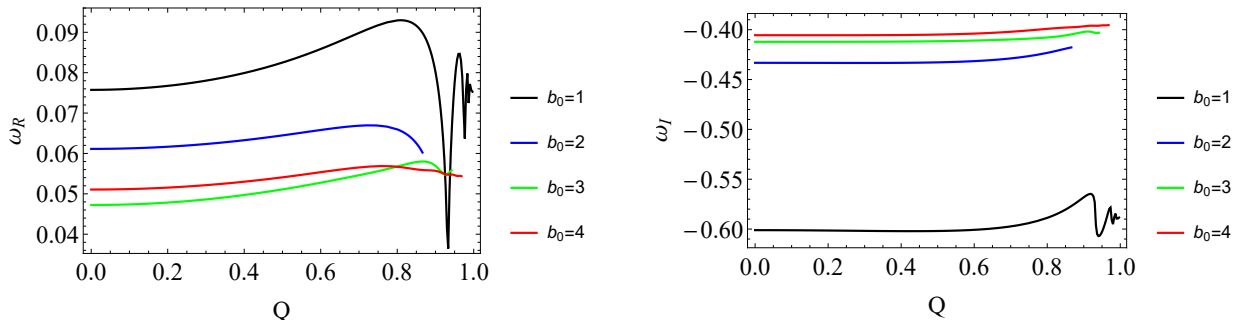


FIG. 10: For massless scalar field, QNFs of the second overtone ($n = 2$) with $l = 0$ are presented as a function of the charge Q for different quantum parameters $b_0 = 1, 2, 3, 4$. The left and right panels show the real and imaginary parts, respectively.

Subsequently, we turn on the multipole quantum number l and analyze the properties of the QNFs. Fig.11 presents the QNFs with $l = 1$ as a function of b_0 for $Q = \frac{2}{5}$. For the fundamental mode ($n = 0$), increasing b_0 results in a monotonic decrease in ω_R and a monotonic increase in ω_I , consistent with the $l = 0$ case. For the first two overtones, ω_R exhibits non-monotonic behavior as a function of b_0 , which is a slower outburst compared to $l = 0$. This is likely due to the activation of the centrifugal potential for non-zero l .

[60, 63, 64], which suppresses the gravitational potential and, consequently, the quantum gravity effect. As discussed in the introduction and previous works [47, 55, 60, 63, 64], this non-monotonic behavior in ω_R is a manifestation of the quantum gravity effect. When the charge parameter Q is increased (see Fig.12 for $Q = \frac{4}{5}$), the non-monotonic behavior in ω_R disappears across the allowed b_0 -rang. We expect that the non-monotonic behaviors and overtone outburst will reemerge at higher overtones, as observed in previous studies [45, 47, 55, 60, 61, 63, 64]. However, the numerical computation of higher overtone modes becomes more challenging in the presence of charge, so we defer this to future work.

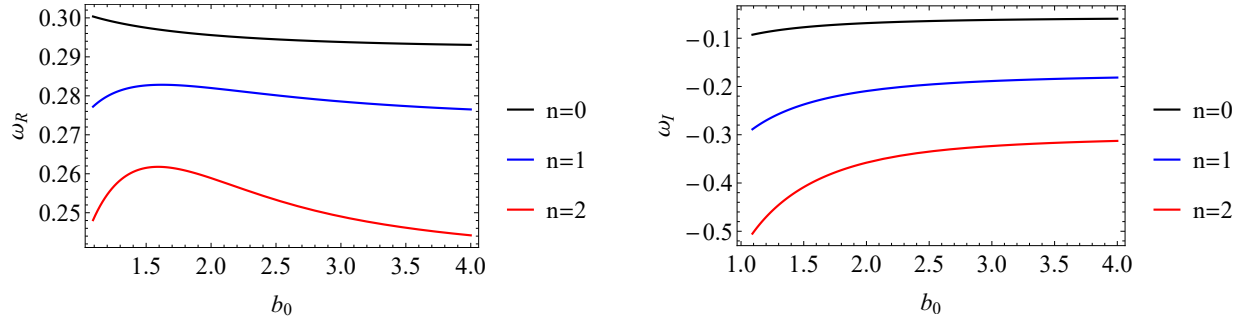


FIG. 11: For massless scalar field, QNFs of fundamental mode and the first two overtones with $l = 1$ are presented as functions of the quantum parameter b_0 for $Q = \frac{2}{5}$. The left and right panels show the real and imaginary parts, respectively.

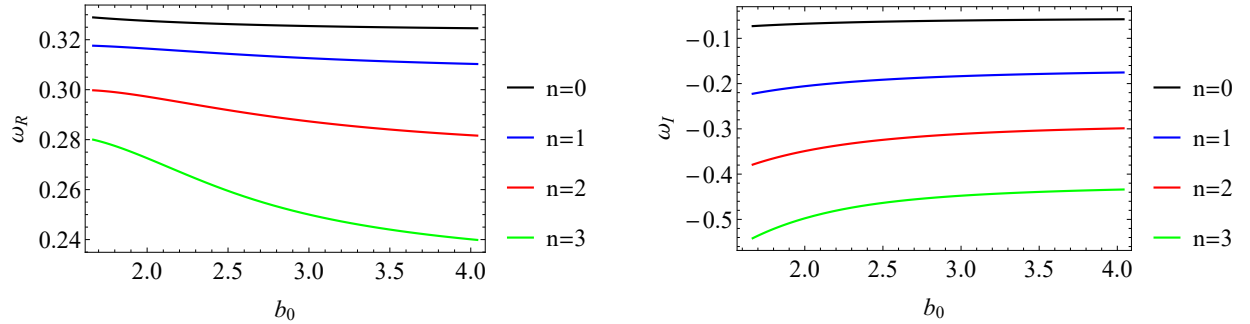


FIG. 12: For massless scalar field, QNFs of fundamental mode and the first three overtones with $l = 1$ are presented as functions of the quantum parameter b_0 for $Q = \frac{4}{5}$. The left and right panels show the real and imaginary parts, respectively.

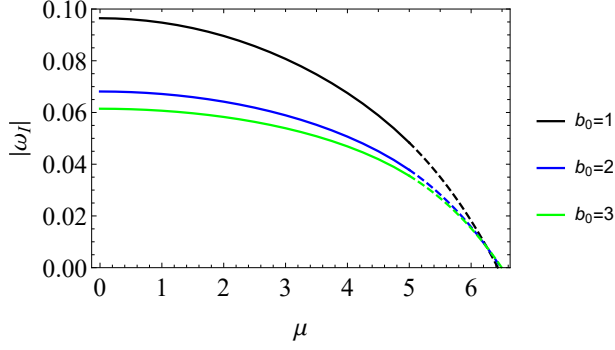


FIG. 13: For massive scalar field, the imaginary parts of the frequencies as function of $\omega(\mu)$, with $l = 20$, $Q = \frac{1}{5}$, $n = 0$, $b_0 = 1, 2, 3$, and $\mu = 0 \dots 6$.

Finally, we activate the mass term to investigate its impact on the QNFs. Given our exclusive focus on the fundamental modes of the massive scalar field, the 6th-order WKB approximation proves sufficient for calculating the QNFs. In addition, we set $l = 20$ here, where the WKB approximation can achieve high accuracy. Fig.13 displays the absolute value of the imaginary parts of the QNFs $|\omega_I|$ as a function of the scalar field mass μ , with fixed charge $Q = \frac{1}{5}$, across varying values of the LQG-correction parameter b_0 . A key observation is the smooth monotonic decrease of $|\omega_I|$ with increasing μ , asymptotically approaching zero. This implies that the decay rate of the modes diminishes as the scalar field mass grows, illustrating the potential for the emergence of arbitrarily long-lived modes. Consequently, massive modes exhibit slower scattering compared to massless modes, and under specific conditions, the oscillations of massive fields become undamped—a phenomenon termed quasi-resonances [105–107]. This behavior is consistent with observations in the neutral ABBV BH [64]. Notably, quasi-resonances have also been reported in Schwarzschild-like brane-localized black hole backgrounds [108], and massive fields with non-zero spin [109, 110]. Importantly, the existence of quasi-resonances is not universal across all spacetime geometries. For instance, they are absent in Schwarzschild-de Sitter spacetimes [106].

B. Dirac field case

In this subsection, we analyze the QNMs of the Dirac field in the charged ABBV BH spacetime using the PSM. As mentioned in the introduction, the study of the overtone modes of the Dirac field is still absent even in the neutral ABBV BH. As a cross-validation, we also

employ 6th order WKB approximation to work out the fundamental modes (see Appendix A for error analysis). In addition, in this subsection, we restrict our focus to the lowest admissible multipole quantum number for spin- $\frac{1}{2}$, i.e., $k = 1$.

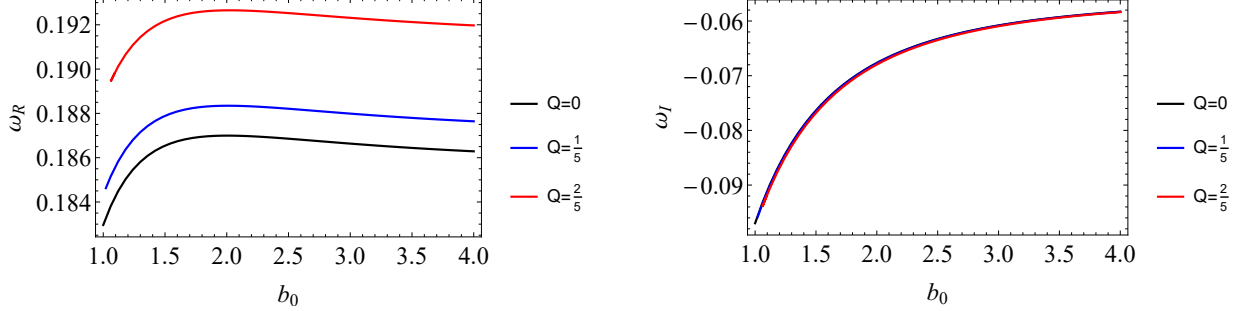


FIG. 14: For Dirac field, QNFs of fundamental modes are presented as a function of the quantum parameter b_0 for $k = 1$, while considering various values of the charge, specifically $Q = 0, \frac{1}{5}, \frac{2}{5}$.

Fig.14 illustrates the QNFs of the Dirac field as a function of the LQG-corrected parameter b_0 , with fixed charge Q . Notably, the real part of the QNFs ω_R manifests a pronounced non-monotonic dependence on b_0 , characterized by an initial increase followed by a gradual decline. This pattern is qualitatively similar to the ω_R behavior in the neutral ABBV BH spacetime (the black curve for $Q = 0$ and also see Ref. [64]). In contrast, the scalar field case displays monotonically decreasing behavior across the same b_0 range ($l = 0$; see left panel of Fig.5). Meanwhile, the imaginary part ω_I demonstrates monotonically increasing magnitudes with b_0 , exhibiting significantly greater variation compared to the RN BH baseline. This amplification of ω_I 's sensitivity to LQG corrections aligns with the scalar field behavior (right panel of Fig. 5), suggesting a potential universality in how quantum-gravity-induced modifications diminish damping rates across scalar and Dirac perturbations.

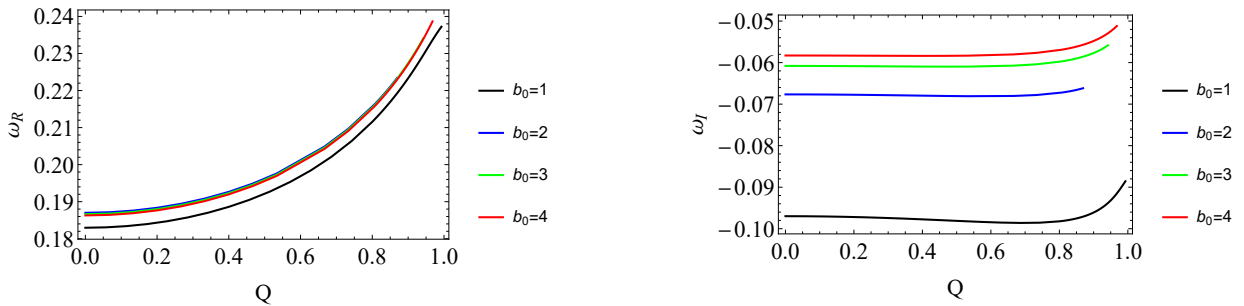


FIG. 15: For Dirac field, QNFs of fundamental modes are presented as a function of the charge Q for $k = 1$, while considering various values of the quantum parameter, specifically $b_0 = 1, 2, 3, 4$.

Fig.15 depicts the QNFs of the Dirac field as functions of the charge Q . The real part of the QNFs ω_R displays a strict monotonic increase with Q , while the imaginary part ω_I remains approximately constant across the majority of the Q -range, deviating only through a subtle upward trend at large Q . This qualitative agreement with the scalar field's QNF behavior under LQG corrections (right panel of Fig. 6) suggests a universal response of scalar and Dirac perturbations to charge-dependent quantum spacetime modifications. Notably, even in the RN limit ($b_0 = 1$), the dependence of the ω_R on Q for Dirac field is strictly monotonic (black curve in the left panel of Fig.15). This behavior stands in sharp contrast to the scalar field's non-monotonic Q -dependence observed under identical RN limit (see black curve for $b_0 = 1$ in the left panel of Fig.6).

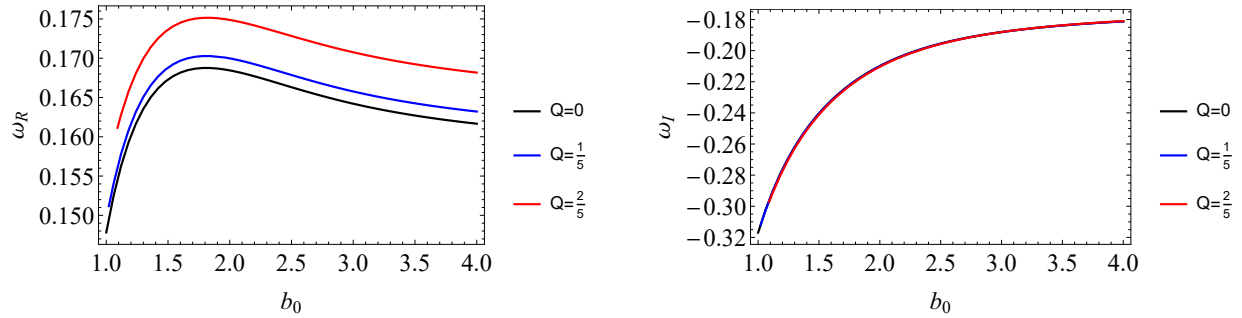


FIG. 16: For Dirac field, QNFs of the first overtone ($n = 1$) with $k = 1$ are presented as a function of the quantum parameter b_0 for the values of the charge $Q = 0, \frac{1}{5}, \frac{2}{5}$. The left and right panels show the real and imaginary parts, respectively.

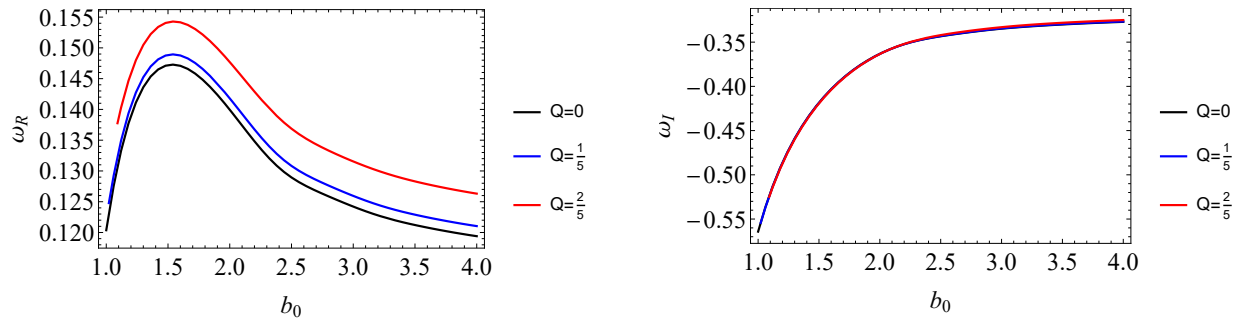


FIG. 17: For Dirac field, QNFs of the second overtone ($n = 2$) with $k = 1$ are presented as a function of the quantum parameter b_0 for the values of the charge $Q = 0, \frac{1}{5}, \frac{2}{5}$. The left and right panels show the real and imaginary parts, respectively.

We now investigate the overtone spectra of the Dirac field. Fig.16 ($n = 1$) and Fig.17 ($n = 2$) display the QNFs as functions of the quantum parameter b_0 for varying charge

Q . A key observation is the enhanced non-monotonicity of ω_R in overtones compared to fundamental modes ($n = 0$), although no pronounced outbursts or oscillatory patterns emerge in the first two overtones. This contrasts with the scalar field dynamics for the lowest admissible multipole quantum number ($l = 0$), where quantum gravity effects induce both overtone outbursts and oscillatory behavior. However, we note that for the scalar field with $l = 1$, these outbursts and oscillatory patterns are also replaced by non-monotonic behavior. We hypothesize that similar outbursts or oscillatory patterns may reemerge in the Dirac field at higher overtones, a possibility we reserve for future investigation. Notably, the imaginary part ω_I retains its monotonic growth with b_0 , consistent with the behavior observed in fundamental modes.

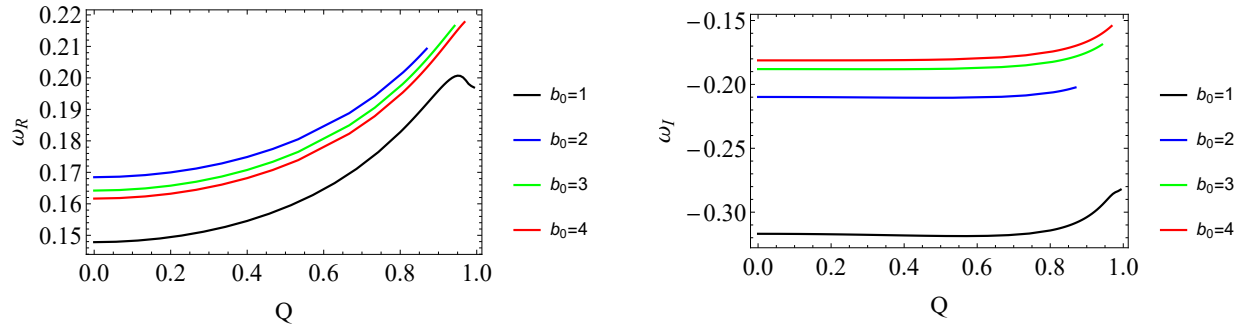


FIG. 18: For Dirac field, QNFs of the first overtone ($n = 1$) with $k = 1$ are presented as a function of the charge Q for different quantum parameters $b_0 = 1, 2, 3, 4$. The left and right panels show the real and imaginary parts, respectively.

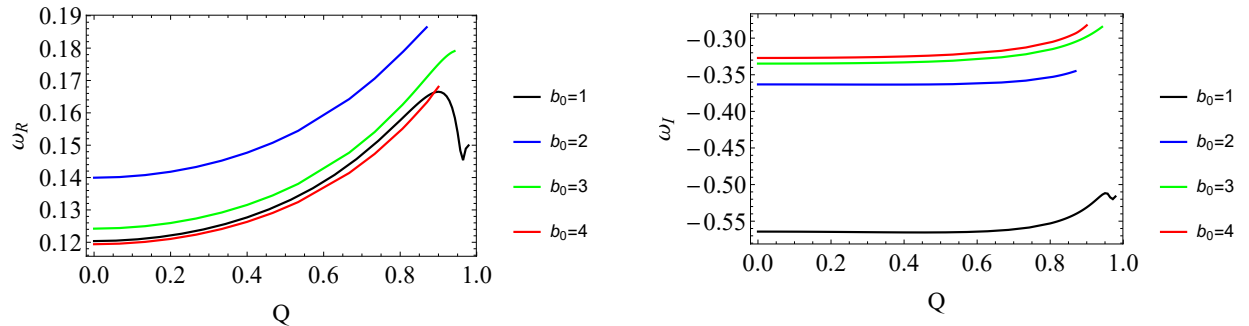


FIG. 19: For Dirac field, QNFs of the second overtone ($n = 2$) with $k = 1$ are presented as a function of the charge Q for different quantum parameters $b_0 = 1, 2, 3, 4$. The left and right panels show the real and imaginary parts, respectively.

Fig.18 ($n = 1$) and Fig.19 ($n = 2$) exhibit the QNFs as functions of charge Q under fixed quantum parameter b_0 . In the RN BH limit ($b_0 = 1$), we observe a clear non-monotonic

dependence of ω_R on Q for $n = 1$ as $Q \rightarrow 1$. This non-monotonicity transitions into a weak amplitude outburst and oscillatory pattern for $n = 2$. But the outburst and oscillatory is weaker than their scalar field counterparts with $l = 0$ (cf. Subsection III A). Remarkably, when quantum corrections are activated ($b_0 > 1$), all anomalous features – non-monotonicity, outbursts, and oscillations – are entirely suppressed for the first two overtones across the allowed Q -range. This suppression effect aligns with our earlier findings in the scalar field case, suggesting a universal interplay between charge Q and quantum parameter b_0 .

IV. CONCLUSIONS AND DISCUSSIONS

In this work, we have systematically analyzed the properties of the QNM spectra of massless/massive scalar and Dirac fields around a charged ABBV BH, unveiling novel signatures of quantum gravity effects and their interplay with the charge. Our key findings and their implications are summarized as follows:

- The LQG-corrected parameter b_0 triggers a distinct overtone outburst in the QNM spectra, particularly pronounced for the scalar field with $l = 0$. This outburst, usually accompanying with an oscillatory pattern, grow more pronounced with increasing overtone numbers, marking a direct imprint of quantum gravity effect on the BH spectroscopy. For the scalar field with $l > 0$ and the Dirac field, however, the overtone outburst develops more slowly or degenerates into non-monotonic on b_0 , suggesting a competition between quantum corrections and centrifugal potential barriers. These anomalies provide a unique spectral fingerprint to observationally discriminate LQG-BHs from their classical counterparts.
- Increasing the charge parameter Q universally suppresses quantum-gravity-induced spectral features—outbursts, non-monotonicity, and oscillations.
- Our findings provide evidence for the existence of quasi-resonances in the massive scalar QNM spectrum, highlighting the potential for the occurrence of arbitrarily long-lived modes in this charged LQG spacetime.

Future studies should extend this work to rotating LQG-BHs (e.g., quantum Kerr analogs), where frame-dragging and ergoregion instabilities may amplify quantum spectral

features. Further, a deeper understanding of the physical mechanism behind the overtone outburst and the role of different parameters in governing this phenomenon could shed light on new physics beyond GR.

Acknowledgments

We would like to express our sincere gratitude to the anonymous reviewer for the insightful and valuable suggestions. We are especially grateful to Prof. Rui-Hong Yue for helpful discussions and suggestions. This work is supported by National Key R&D Program of China (No. 2020YFC2201400), the Natural Science Foundation of China under Grants No. 12375055, 12347159 and 12447151.

Appendix A: Error analysis

To establish the numerical fidelity of our PSM-based QNM calculations, we perform a systematic cross-validation against the WKB approximation, focusing on fundamental modes ($n = 0$) and low overtones ($n \leq 2$).

The WKB method — a semi-analytical approach requiring only the maximum value of the effective potential $V_{\text{eff}}(r_*)$ and its derivatives — provides an efficient QNF calculating method for $n < l$. The general WKB formula could be written as:

$$\begin{aligned} \omega^2 = & V_0 + A_2(\mathcal{K}^2) + A_4(\mathcal{K}^2) + A_6(\mathcal{K}^2) + \dots \\ & - i\mathcal{K}\sqrt{-2V_2}(1 + A_3(\mathcal{K}^2) + A_5(\mathcal{K}^2) + A_7(\mathcal{K}^2) + \dots), \end{aligned} \quad (\text{A1})$$

where $\mathcal{K} = n + 1/2$ is half-integer. The correction terms $A_k(\mathcal{K}^2)$ are polynomials of \mathcal{K}^2 whose rational coefficients depend on higher-order derivatives of $V_{\text{eff}}(r_*)$ at its maximum. For computational robustness, we employ the 13th WKB with Padé approximation [111] for massless scalar fields and the sixth-order WKB approximation to calculate the QNFs, respectively.

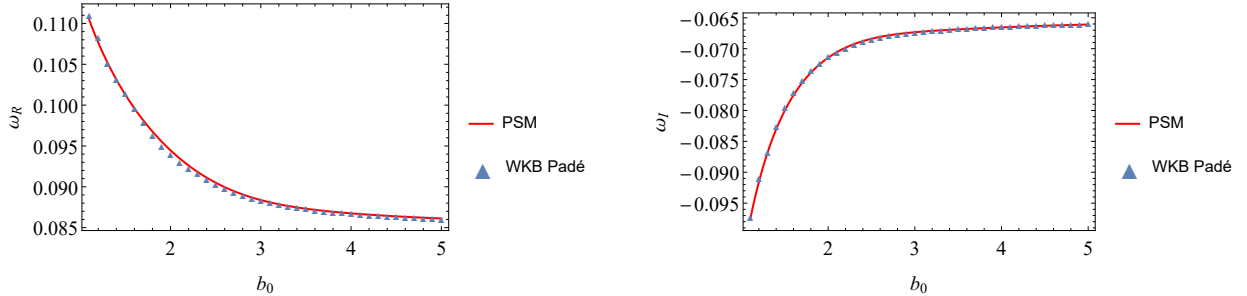


FIG. 20: QNFs of the massless scalar field as functions of the quantum parameter b_0 , computed via PSM and 13th WKB approximation with Padé approximation. Here, $Q = \frac{2}{5}, l = 0, n = 0$.

Fig.20, Fig.21 and Fig.22 show PSM-computed QNFs against WKB predictions for massless scalar field with $l = 0, n = 0$ (Fig.20) and $l = 1, n = 0, 1, 2$ (Fig.21), and Dirac field with $l = 1, n = 0$ (Fig.22). Qualitatively, the spectral overlap between PSM and WKB is striking across all cases. To quantify this concordance, we define the relative percentage deviations:

$$\varepsilon_{Re} = \left| \frac{\omega_{PS}^{Re} - \omega_{WKB}^{Re}}{\omega_{PS}^{Re}} \right| \times 100\%, \quad \varepsilon_{Im} = \left| \frac{\omega_{PS}^{Im} - \omega_{WKB}^{Im}}{\omega_{PS}^{Im}} \right| \times 100\%. \quad (\text{A2})$$

Here, ε_{Re} and ε_{Im} denote the percentage deviations in the real and imaginary parts of the

QNFs, respectively. These metrics are computed relative to the PSM results, which serve as the reference standard for this comparison.

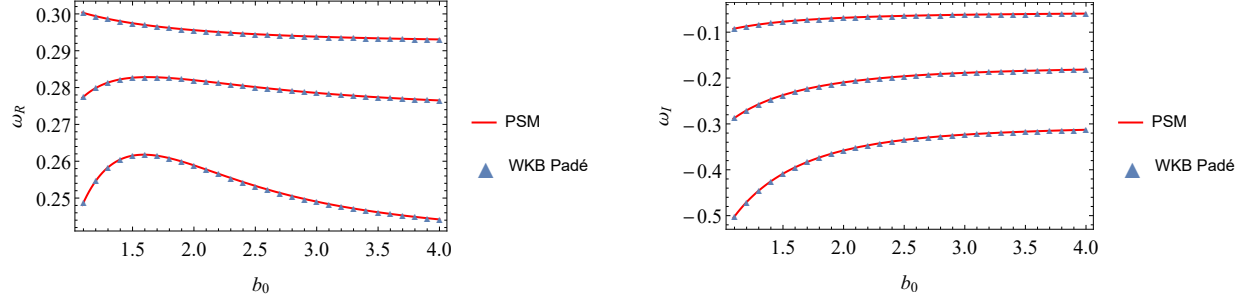


FIG. 21: QNFs of the massless scalar field as functions of the quantum parameter b_0 , computed via PSM and 13^{th} WKB approximation with Padé approximation. Here, $Q = \frac{2}{5}$, $l = 1$ and $n = 0, 1, 2$ (from top to bottom).

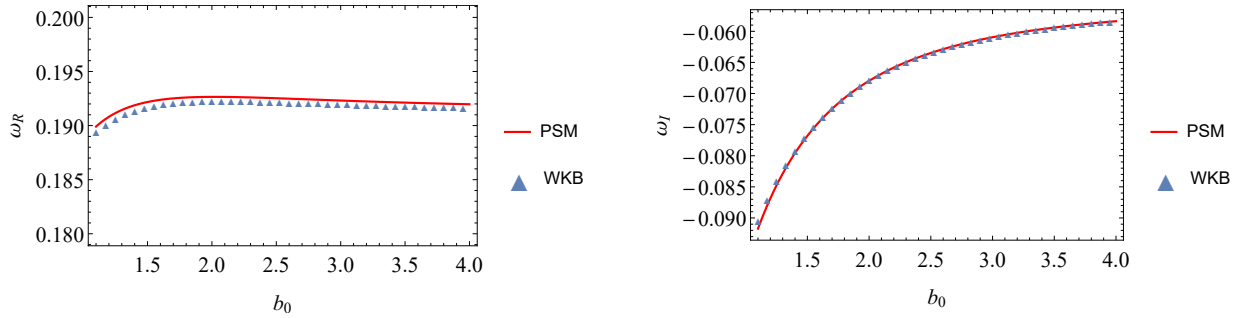


FIG. 22: QNFs of the Dirac field as functions of the quantum parameter b_0 , computed via PSM and sixth-order WKB approximation. Here, $Q = \frac{2}{5}$, $k = 1$, $n = 0$.

Tables I–III detail the deviations $\varepsilon_{Re/Im}$ for fixed Q and various values of b_0 . Key findings:

- **Massless scalar field with $l = 0, n = 0$:** $\varepsilon_{Re/Im} \lesssim 10^{-1}\%$,
- **Massless scalar field with $l = 1, n = 0$:** $\varepsilon_{Re/Im} < 10^{-4}\%$,
- **Dirac field with $k = 1, n = 0$:** $\varepsilon_{Re/Im} \lesssim 1\%$.

The strong consistency between the WKB and PSM results underscores the reliability of our PSM-based QNM calculations. This agreement serves as a critical cross-verification, highlighting the robustness of PSM-based QNM analysis in this work.

Q	b_0	ω_{PSM}	$\omega_{\text{WKB Padé}}$	$\varepsilon_{Re} (\%)$	$\varepsilon_{Im} (\%)$
2/5	1.1	0.110431 - 0.0976727 <i>i</i>	0.111010 - 0.0973977 <i>i</i>	0.5243	0.2815
	1.5	0.101271 - 0.0800035 <i>i</i>	0.101383 - 0.0795293 <i>i</i>	0.1105	0.5927
	2	0.0944658 - 0.0714582 <i>i</i>	0.0939013 - 0.0713471 <i>i</i>	0.5976	0.1556
	2.5	0.0905033 - 0.0683967 <i>i</i>	0.0903154 - 0.0684605 <i>i</i>	0.2076	0.0933
	3	0.0883746 - 0.0673379 <i>i</i>	0.0883085 - 0.0673566 <i>i</i>	0.0748	0.0279
	3.5	0.0873154 - 0.0668779 <i>i</i>	0.0872944 - 0.0667929 <i>i</i>	0.0241	0.1271
	4	0.0867482 - 0.0665548 <i>i</i>	0.0866981 - 0.0664276 <i>i</i>	0.0578	0.1912

TABLE I: Comparison of the relative errors $\varepsilon_{Re/Im}$ in the QNFs for a massless scalar field, computed via PSM and 13th WKB method with Padé approximation, for various b_0 with $Q = \frac{2}{5}$, $l = 0$ and $n = 0$.

Q	b_0	ω_{PSM}	$\omega_{\text{WKB Padé}}$	$\varepsilon_{Re} (\%)$	$\varepsilon_{Im} (\%)$
2/5	1.1	0.300270 - 0.0922177 <i>i</i>	0.300270 - 0.0922177 <i>i</i>	0	0
	1.5	0.297472 - 0.0772634 <i>i</i>	0.297472 - 0.0772634 <i>i</i>	0	0
	2	0.295583 - 0.0686968 <i>i</i>	0.295583 - 0.0686968 <i>i</i>	0	0
	2.5	0.294495 - 0.0644370 <i>i</i>	0.294495 - 0.0644371 <i>i</i>	0	0
	3	0.293819 - 0.0620358 <i>i</i>	0.293819 - 0.0620358 <i>i</i>	0	0
	3.5	0.293374 - 0.0605580 <i>i</i>	0.293374 - 0.0605580 <i>i</i>	0	0
	4	0.293069 - 0.0595871 <i>i</i>	0.293069 - 0.0595871 <i>i</i>	0	0

TABLE II: Comparison of the relative errors $\varepsilon_{Re/Im}$ in the QNFs for a massless scalar field, computed via PSM and 13th WKB method with Padé approximation, for various b_0 with $Q = \frac{2}{5}$, $l = 1$ and $n = 0$. An error of 0% indicates that the difference is smaller than $10^{-4}\%$.

Q	b_0	ω_{PSM}	ω_{WKB}	$\varepsilon_{Re} (\%)$	$\varepsilon_{Im} (\%)$
2/5	1.1	0.189906 - 0.0917185 <i>i</i>	0.189393 - 0.0905825 <i>i</i>	0.2705	1.2386
	1.5	0.192179 - 0.0768029 <i>i</i>	0.191661 - 0.0766089 <i>i</i>	0.2694	0.2526
	2	0.192652 - 0.0679596 <i>i</i>	0.192230 - 0.0679397 <i>i</i>	0.2194	0.0294
	2.5	0.192527 - 0.0634864 <i>i</i>	0.192144 - 0.0634900 <i>i</i>	0.1992	0.0056
	3	0.192314 - 0.0609546 <i>i</i>	0.191948 - 0.0609694 <i>i</i>	0.1899	0.0242
	3.5	0.192123 - 0.0593985 <i>i</i>	0.191769 - 0.0594200 <i>i</i>	0.1841	0.0361
	4	0.191971 - 0.0583792 <i>i</i>	0.191625 - 0.0584046 <i>i</i>	0.1804	0.0435

TABLE III: Comparison of the relative errors $\varepsilon_{Re/Im}$ in the QNFs for a Dirac field, computed via PSM and sixth-order WKB method, for various b_0 with $Q = \frac{2}{5}$, $k = 1$ and $n = 0$.

Appendix B: The reduced wave equations

By imposing the appropriate boundary conditions, the wave equation (11) reduces to the following form:

$$\alpha_0 \psi'' + \beta_0 \psi' + \gamma_0 \psi = 0, \quad (\text{B1})$$

where the coefficients are determined by the specific field under consideration. For the massless scalar field, the coefficients are given by:

$$\alpha_0 = 2b_0^4 u^2 f(u) (m - r_0 g(u)), \quad (\text{B2})$$

$$\begin{aligned} \beta_0 = & ib_0^2 u^2 f(u) [-8(m - r_0 \omega g(u)) (-mu + b_0^2 r_h + 3b_0^2 mu) \omega + ib_0^2 r_0 u^2 g'(u)] \\ & + 2b_0^4 u^2 [2i\sqrt{m} r_h \omega \sqrt{m - r_0 g(u)} + u^2 (m - r_0 g(u)) f'(u)], \end{aligned} \quad (\text{B3})$$

$$\begin{aligned} \gamma_0 = & 2ib_0^2 u^2 [-mu + b_0^2 (r_h + 3mu)] \omega (m - r_0 g(u)) f'(u) - ib_0^2 r_0 u^2 (-mu + b_0^2 r_h + 3b_0^2 mu) g'(u) \\ & + b_0^2 \sqrt{m} \left\{ b_0^2 (l^2 + l) \sqrt{m} u^2 + [4mr_h u \omega^2 - 2r_h \omega (-iu + 2r_h \omega + 6mu\omega)] \sqrt{m - r_0 g(u)} \right\} \\ & + \{ 2m^2 u [2mu\omega + b_0^2 (-4r_h \omega + iu - 12mu\omega)] + b_0^4 [2r_h^2 \omega - u (2r_h + 3mu) (i - 6m\omega)] \} \\ & (\omega f(u) - 2r_0 g(u)). \end{aligned} \quad (\text{B4})$$

For the Dirac field, the coefficients are:

$$\alpha_0 = -2u(1-u^2)^4 f(u)^2 b_0^4 (m - g(u) r_0) , \quad (\text{B5})$$

$$\begin{aligned} \beta_0 = & \left\{ b_0^2 (u^2 - 1)^2 [-2u f'(u) (m - r_0 g(u)) + f(u) r_0 (u g'(u) - 2g(u)) + 2f(u)m] \right. \\ & \left. + 8im b_0^2 u^2 \omega r_h \sqrt{1 - \frac{r_0 g(u)}{m}} + 16iu^2 \omega f(u) [-b_0^2 (r_h - 3u^2 + 3) - u^2 + 1] (m - r_0 g(u)) \right\} \\ & \times b_0^2 f(u) (1 - u^2)^2 , \end{aligned} \quad (\text{B6})$$

$$\begin{aligned} \gamma_0 = & \left\{ 4u^2 \omega (b_0^2 (r_h - 3u^2 + 3) + u^2 - 1)^2 + ib_0^2 (u^2 - 1) \{ b_0^2 [(3u^2 + 1) r_h - 3u^4 + 3] + u^4 - 1 \} \right. \\ & \times 8u \omega f(u)^2 (m - r_0 g(u)) \\ & + \left\{ f(u) \left\{ -2(u^2 - 1) [(u^2 - 1) f'(u) (m - r_0 g(u)) + 2k^2 m u] + 8im u \omega r_h \sqrt{1 - \frac{r_0 g(u)}{m}} \right\} + \right. \\ & \left. km(u^2 - 1)^2 \sqrt{f(u)} f'(u) \sqrt{1 - \frac{r_0 g(u)}{m}} + r(u^2 - 1)^2 \left[r_0 f(u)^2 g'(u) + 4k m u f(u)^{3/2} \sqrt{1 - \frac{r_0 g(u)}{m}} \right] \right\} \\ & \times 2b_0^4 u^2 (1 - u^2) \\ & + \left\{ -2(u^2 - 1)^2 u f'(u) (m - r_0 g(u)) + (u^2 - 1)^2 f(u) [r_0 (u g'(u) - 2g(u)) + 2m] \right. \\ & \left. + 8im u^2 \omega r_h \sqrt{1 - \frac{r_0 g(u)}{m}} \right\} \times (b_0^2 (r_h - 3u^2 + 3) + u^2 - 1) \\ & \times 4ib_0^2 u \omega f(u) . \end{aligned} \quad (\text{B7})$$

-
- [1] C. Rovelli, *Quantum Gravity*, Cambridge University Press, Cambridge, UK (2004).
 - [2] T. Thiemann, *Modern canonical quantum general relativity*, [gr-qc/0110034](#).
 - [3] A. Ashtekar and J. Lewandowski, *Background independent quantum gravity: A Status report*, *Class. Quant. Grav.* **21** (2004) R53, [[gr-qc/0404018](#)].
 - [4] M. Han, W. Huang, and Y. Ma, *Fundamental structure of loop quantum gravity*, *Int. J. Mod. Phys. D* **16** (2007) 1397–1474, [[gr-qc/0509064](#)].
 - [5] M. Bojowald, *Absence of singularity in loop quantum cosmology*, *Phys. Rev. Lett.* **86** (2001) 5227–5230, [[gr-qc/0102069](#)].

- [6] A. Ashtekar, T. Pawłowski, and P. Singh, *Quantum nature of the big bang*, Phys. Rev. Lett. **96** (2006) 141301, [[gr-qc/0602086](#)].
- [7] A. Ashtekar, T. Pawłowski, and P. Singh, *Quantum Nature of the Big Bang: An Analytical and Numerical Investigation. I.*, Phys. Rev. D **73** (2006) 124038, [[gr-qc/0604013](#)].
- [8] A. Ashtekar, T. Pawłowski, and P. Singh, *Quantum Nature of the Big Bang: Improved dynamics*, Phys. Rev. D **74** (2006) 084003, [[gr-qc/0607039](#)].
- [9] A. Ashtekar, M. Bojowald, and J. Lewandowski, *Mathematical structure of loop quantum cosmology*, Adv. Theor. Math. Phys. **7** (2003), no. 2 233–268, [[gr-qc/0304074](#)].
- [10] M. Bojowald, *Loop quantum cosmology*, Living Rev. Rel. **8** (2005) 11, [[gr-qc/0601085](#)].
- [11] A. Ashtekar and P. Singh, *Loop Quantum Cosmology: A Status Report*, Class. Quant. Grav. **28** (2011) 213001, [[arXiv:1108.0893](#)].
- [12] E. Wilson-Ewing, *Testing loop quantum cosmology*, Comptes Rendus Physique **18** (2017) 207–225, [[arXiv:1612.04551](#)].
- [13] M. Bojowald, G. Date, and K. Vandersloot, *Homogeneous loop quantum cosmology: The Role of the spin connection*, Class. Quant. Grav. **21** (2004) 1253–1278, [[gr-qc/0311004](#)].
- [14] P. Singh and A. Toporensky, *Big crunch avoidance in $K=1$ semiclassical loop quantum cosmology*, Phys. Rev. D **69** (2004) 104008, [[gr-qc/0312110](#)].
- [15] G. V. Vereshchagin, *Qualitative approach to semi-classical loop quantum cosmology*, JCAP **07** (2004) 013, [[gr-qc/0406108](#)].
- [16] G. Date, *Absence of the Kasner singularity in the effective dynamics from loop quantum cosmology*, Phys. Rev. D **71** (2005) 127502, [[gr-qc/0505002](#)].
- [17] G. Date and G. M. Hossain, *Genericity of big bounce in isotropic loop quantum cosmology*, Phys. Rev. Lett. **94** (2005) 011302, [[gr-qc/0407074](#)].
- [18] R. Goswami, P. S. Joshi, and P. Singh, *Quantum evaporation of a naked singularity*, Phys. Rev. Lett. **96** (2006) 031302, [[gr-qc/0506129](#)].
- [19] T. Papanikolaou, *Primordial black holes in loop quantum cosmology: the effect on the threshold*, Class. Quant. Grav. **40** (2023), no. 13 134001, [[arXiv:2301.11439](#)].
- [20] M. Bojowald, *The Early universe in loop quantum cosmology*, J. Phys. Conf. Ser. **24** (2005) 77–86, [[gr-qc/0503020](#)].
- [21] T. Stachowiak and M. Szydlowski, *Exact solutions in bouncing cosmology*, Phys. Lett. B **646** (2007) 209–214, [[gr-qc/0610121](#)].

- [22] A. Ashtekar and M. Bojowald, *Quantum geometry and the Schwarzschild singularity*, Class. Quant. Grav. **23** (2006) 391–411, [[gr-qc/0509075](#)].
- [23] C. G. Boehmer and K. Vandersloot, *Loop Quantum Dynamics of the Schwarzschild Interior*, Phys. Rev. D **76** (2007) 104030, [[arXiv:0709.2129](#)].
- [24] D.-W. Chiou, *Phenomenological loop quantum geometry of the Schwarzschild black hole*, Phys. Rev. D **78** (2008) 064040, [[arXiv:0807.0665](#)].
- [25] A. Perez, *Black Holes in Loop Quantum Gravity*, Rept. Prog. Phys. **80** (2017), no. 12 126901, [[arXiv:1703.09149](#)].
- [26] X. Zhang, *Loop Quantum Black Hole*, Universe **9** (2023), no. 7 313, [[arXiv:2308.10184](#)].
- [27] L. Modesto, *Loop quantum black hole*, Class. Quant. Grav. **23** (2006) 5587–5602, [[gr-qc/0509078](#)].
- [28] L. Modesto, *Semiclassical loop quantum black hole*, Int. J. Theor. Phys. **49** (2010) 1649–1683, [[arXiv:0811.2196](#)].
- [29] M. Campiglia, R. Gambini, and J. Pullin, *Loop quantization of spherically symmetric midi-superspaces*, Class. Quant. Grav. **24** (2007) 3649–3672, [[gr-qc/0703135](#)].
- [30] M. Bojowald and S. Brahma, *Signature change in two-dimensional black-hole models of loop quantum gravity*, Phys. Rev. D **98** (2018), no. 2 026012, [[arXiv:1610.08850](#)].
- [31] A. Joe and P. Singh, *Kantowski-Sachs spacetime in loop quantum cosmology: bounds on expansion and shear scalars and the viability of quantization prescriptions*, Class. Quant. Grav. **32** (2015), no. 1 015009, [[arXiv:1407.2428](#)].
- [32] D.-W. Chiou, *Phenomenological dynamics of loop quantum cosmology in Kantowski-Sachs spacetime*, Phys. Rev. D **78** (2008) 044019, [[arXiv:0803.3659](#)].
- [33] R. Gambini, J. Olmedo, and J. Pullin, *Spherically symmetric loop quantum gravity: analysis of improved dynamics*, Class. Quant. Grav. **37** (2020), no. 20 205012, [[arXiv:2006.01513](#)].
- [34] J. G. Kelly, R. Santacruz, and E. Wilson-Ewing, *Effective loop quantum gravity framework for vacuum spherically symmetric spacetimes*, Phys. Rev. D **102** (2020), no. 10 106024, [[arXiv:2006.09302](#)].
- [35] V. Husain, J. G. Kelly, R. Santacruz, and E. Wilson-Ewing, *Fate of quantum black holes*, Phys. Rev. D **106** (2022), no. 2 024014, [[arXiv:2203.04238](#)].
- [36] M. Han and H. Liu, *Covariant $\bar{\mu}$ -scheme effective dynamics, mimetic gravity, and non-singular black holes: Applications to spherical symmetric quantum gravity and CGHS*

- model, [arXiv:2212.04605](#).
- [37] A. Corichi and P. Singh, *Loop quantization of the Schwarzschild interior revisited*, Class. Quant. Grav. **33** (2016), no. 5 055006, [[arXiv:1506.08015](#)].
 - [38] J. Olmedo, S. Saini, and P. Singh, *From black holes to white holes: a quantum gravitational, symmetric bounce*, Class. Quant. Grav. **34** (2017), no. 22 225011, [[arXiv:1707.07333](#)].
 - [39] A. Ashtekar, J. Olmedo, and P. Singh, *Quantum Transfiguration of Kruskal Black Holes*, Phys. Rev. Lett. **121** (2018), no. 24 241301, [[arXiv:1806.00648](#)].
 - [40] A. Ashtekar, J. Olmedo, and P. Singh, *Quantum extension of the Kruskal spacetime*, Phys. Rev. D **98** (2018), no. 12 126003, [[arXiv:1806.02406](#)].
 - [41] J. Lewandowski, Y. Ma, J. Yang, and C. Zhang, *Quantum Oppenheimer-Snyder and Swiss Cheese Models*, Phys. Rev. Lett. **130** (2023), no. 10 101501, [[arXiv:2210.02253](#)].
 - [42] R. A. Konoplya and A. Zhidenko, *First few overtones probe the event horizon geometry*, JHEAp **44** (2024) 419–426, [[arXiv:2209.00679](#)].
 - [43] E. Berti, V. Cardoso, and C. M. Will, *On gravitational-wave spectroscopy of massive black holes with the space interferometer LISA*, Phys. Rev. D **73** (2006) 064030, [[gr-qc/0512160](#)].
 - [44] E. Berti, K. Yagi, H. Yang, and N. Yunes, *Extreme Gravity Tests with Gravitational Waves from Compact Binary Coalescences: (II) Ringdown*, Gen. Rel. Grav. **50** (2018), no. 5 49, [[arXiv:1801.03587](#)].
 - [45] G. Fu, D. Zhang, P. Liu, X.-M. Kuang, Q. Pan, and J.-P. Wu, *Quasinormal modes and Hawking radiation of a charged Weyl black hole*, Phys. Rev. D **107** (2023), no. 4 044049, [[arXiv:2207.12927](#)].
 - [46] G. Fu, D. Zhang, P. Liu, X.-M. Kuang, and J.-P. Wu, *Peculiar properties in quasinormal spectra from loop quantum gravity effect*, Phys. Rev. D **109** (2024), no. 2 026010, [[arXiv:2301.08421](#)].
 - [47] H. Gong, S. Li, D. Zhang, G. Fu, and J.-P. Wu, *Quasinormal modes of quantum-corrected black holes*, [arXiv:2312.17639](#).
 - [48] F. Moura and J. a. Rodrigues, *Eikonal quasinormal modes and shadow of string-corrected d-dimensional black holes*, Phys. Lett. B **819** (2021) 136407, [[arXiv:2103.09302](#)].
 - [49] F. Moura and J. a. Rodrigues, *Asymptotic quasinormal modes of string-theoretical d-dimensional black holes*, JHEP **08** (2021) 078, [[arXiv:2105.02616](#)].
 - [50] F. Moura and J. a. Rodrigues, *The isospectrality of asymptotic quasinormal modes of large*

- Gauss-Bonnet d-dimensional black holes*, Nucl. Phys. B **993** (2023) 116255, [[arXiv:2206.11377](#)].
- [51] J. Lin, M. Bravo-Gaete, and X. Zhang, *Quasinormal modes, greybody factors, and thermodynamics of four dimensional AdS black holes in critical gravity*, Phys. Rev. D **109** (2024), no. 10 104039, [[arXiv:2401.02045](#)].
 - [52] R. Ghosh, M. Rahman, and A. K. Mishra, *Regularized stable Kerr black hole: cosmic censorship, shadow and quasi-normal modes*, Eur. Phys. J. C **83** (2023), no. 1 91, [[arXiv:2209.12291](#)].
 - [53] R. A. Konoplya, Z. Stuchlik, A. Zhidenko, and A. F. Zinhailo, *Quasinormal modes of renormalization group improved Dymnikova regular black holes*, Phys. Rev. D **107** (2023), no. 10 104050, [[arXiv:2303.01987](#)].
 - [54] A. F. Zinhailo, *Quasinormal spectrum in the asymptotically safe gravity*, 11, 2023. [arXiv:2311.05380](#).
 - [55] D. Zhang, H. Gong, G. Fu, J.-P. Wu, and Q. Pan, *Quasinormal modes of a regular black hole with sub-Planckian curvature*, Eur. Phys. J. C **84** (2024), no. 6 564, [[arXiv:2402.15085](#)].
 - [56] Z. Song, H. Gong, H.-L. Li, G. Fu, L.-G. Zhu, and J.-P. Wu, *Quasinormal modes and ringdown waveform of the Frolov black hole*, [arXiv:2406.04787](#).
 - [57] R. A. Konoplya and O. S. Stashko, *Probing the Effective Quantum Gravity via Quasinormal Modes and Shadows of Black Holes*, [arXiv:2408.02578](#).
 - [58] O. Stashko, *Quasinormal modes and gray-body factors of regular black holes in asymptotically safe gravity*, [arXiv:2407.07892](#).
 - [59] A. Dubinsky and A. F. Zinhailo, *Analytic expressions for grey-body factors of the general parametrized spherically symmetric black holes*, [arXiv:2410.15232](#).
 - [60] A. F. Zinhailo, *Black Hole in the Quantum Oppenheimer-Snyder model: long lived modes and the overtones' behavior*, .
 - [61] Z. Dong, D. Zhang, G. Fu, and J.-P. Wu, *Quasinormal modes of a d-dimensional regular black hole featuring an integrable singularity*, [arXiv:2412.20457](#).
 - [62] E. R. Livine, C. Montagnon, N. Oshita, and H. Roussille, *Scalar Quasi-Normal Modes of a loop quantum black hole*, JCAP **10** (2024) 037, [[arXiv:2405.12671](#)].
 - [63] R. A. Konoplya, A. F. Zinhailo, J. Kunz, Z. Stuchlik, and A. Zhidenko, *Quasinormal*

- ringing of regular black holes in asymptotically safe gravity: the importance of overtones*, JCAP **10** (2022) 091, [[arXiv:2206.14714](#)].
- [64] S. V. Bolokhov, *Long-lived quasinormal modes and overtones' behavior of holonomy-corrected black holes*, Phys. Rev. D **110** (2024), no. 2 024010, [[arXiv:2311.05503](#)].
- [65] A. Corichi, T. Vukasinac, and J. A. Zapata, *Polymer Quantum Mechanics and its Continuum Limit*, Phys. Rev. D **76** (2007) 044016, [[arXiv:0704.0007](#)].
- [66] A. AlonsoBardaji, D. Brizuela, and R. Vera, *An effective model for the quantum Schwarzschild black hole*, Phys. Lett. B **829** (2022) 137075, [[arXiv:2112.12110](#)].
- [67] A. AlonsoBardaji, D. Brizuela, and R. Vera, *Nonsingular spherically symmetric black-hole model with holonomy corrections*, Phys. Rev. D **106** (2022), no. 2 024035, [[arXiv:2205.02098](#)].
- [68] C. Zhang, J. Lewandowski, Y. Ma, and J. Yang, *Black Holes and Covariance in Effective Quantum Gravity*, [arXiv:2407.10168](#).
- [69] R.-T. Chen, S. Li, L.-G. Zhu, and J.-P. Wu, *Constraints from Solar System tests on a covariant loop quantum black hole*, Phys. Rev. D **109** (2024), no. 2 024010, [[arXiv:2311.12270](#)].
- [70] G. Fu, Y. Liu, B. Wang, J.-P. Wu, and C. Zhang, *Probing Quantum Gravity Effects with Eccentric Extreme Mass-Ratio Inspirals*, [arXiv:2409.08138](#).
- [71] T. Zi and S. Kumar, *Eccentric extreme mass-ratio inspirals: A gateway to probe quantum gravity effects*, [arXiv:2409.17765](#).
- [72] A. R. Soares, C. F. S. Pereira, and R. L. L. Vitória, *Holonomy corrected Schwarzschild black hole lensing*, [arXiv:2309.05106](#).
- [73] E. L. B. Junior, F. S. N. Lobo, M. E. Rodrigues, and H. A. Vieira, *Gravitational lens effect of a holonomy corrected Schwarzschild black hole*, [arXiv:2309.02658](#).
- [74] A. E. Balali, *Quantum Schwarzschild Black Hole Optical Aspects*, [arXiv:2310.09829](#).
- [75] Z. S. Moreira, H. C. D. Lima Junior, L. C. B. Crispino, and C. A. R. Herdeiro, *Quasinormal modes of a holonomy corrected Schwarzschild black hole*, Phys. Rev. D **107** (2023), no. 10 104016, [[arXiv:2302.14722](#)].
- [76] D. M. Gingrich, *Quasinormal modes of a nonsingular spherically symmetric black hole effective model with holonomy corrections*, Phys. Rev. D **110** (2024), no. 8 084045,

- [[arXiv:2404.04447](#)].
- [77] A. Alonso-Bardaji, D. Brizuela, and R. Vera, *Singularity resolution by holonomy corrections: Spherical charged black holes in cosmological backgrounds*, Phys. Rev. D **107** (2023), no. 6 064067, [[arXiv:2302.10619](#)].
 - [78] H. A. Borges, I. P. R. Baranov, F. C. Sobrinho, and S. Carneiro, *Remnant loop quantum black holes*, Class. Quant. Grav. **41** (2024), no. 5 05LT01, [[arXiv:2310.01560](#)].
 - [79] D. R. Brill and J. A. Wheeler, *Interaction of neutrinos and gravitational fields*, Rev. Mod. Phys. **29** (1957) 465–479.
 - [80] R. A. Konoplya and A. Zhidenko, *Quasinormal modes of black holes: From astrophysics to string theory*, Rev. Mod. Phys. **83** (2011) 793–836, [[arXiv:1102.4014](#)].
 - [81] A. F. Zinhailo, *Quasinormal modes of Dirac field in the Einstein–Dilaton–Gauss–Bonnet and Einstein–Weyl gravities*, Eur. Phys. J. C **79** (2019), no. 11 912, [[arXiv:1909.12664](#)].
 - [82] E. Berti, V. Cardoso, and A. O. Starinets, *Quasinormal modes of black holes and black branes*, Class. Quant. Grav. **26** (2009) 163001, [[arXiv:0905.2975](#)].
 - [83] K. D. Kokkotas and B. G. Schmidt, *Quasinormal modes of stars and black holes*, Living Rev. Rel. **2** (1999) 2, [[gr-qc/9909058](#)].
 - [84] V. Ferrari and B. Mashhoon, *New approach to the quasinormal modes of a black hole*, Phys. Rev. D **30** (1984) 295–304.
 - [85] B. F. Schutz and C. M. Will, *BLACK HOLE NORMAL MODES: A SEMIANALYTIC APPROACH*, Astrophys. J. Lett. **291** (1985) L33–L36.
 - [86] S. Iyer and C. M. Will, *Black Hole Normal Modes: A WKB Approach. 1. Foundations and Application of a Higher Order WKB Analysis of Potential Barrier Scattering*, Phys. Rev. D **35** (1987) 3621.
 - [87] S. Iyer, *BLACK HOLE NORMAL MODES: A WKB APPROACH. 2. SCHWARZSCHILD BLACK HOLES*, Phys. Rev. D **35** (1987) 3632.
 - [88] R. A. Konoplya, *Quasinormal behavior of the d -dimensional Schwarzschild black hole and higher order WKB approach*, Phys. Rev. D **68** (2003) 024018, [[gr-qc/0303052](#)].
 - [89] J. Matyjasek and M. Opala, *Quasinormal modes of black holes. The improved semianalytic approach*, Phys. Rev. D **96** (2017), no. 2 024011, [[arXiv:1704.00361](#)].
 - [90] H. Ciftci, R. L. Hall, and N. Saad, *Perturbation theory in a framework of iteration methods*, Phys. Lett. A **340** (2005) 388–396, [[math-ph/0504056](#)].

- [91] H. T. Cho, A. S. Cornell, J. Doukas, and W. Naylor, *Black hole quasinormal modes using the asymptotic iteration method*, Class. Quant. Grav. **27** (2010) 155004, [[arXiv:0912.2740](#)].
- [92] H. T. Cho, A. S. Cornell, J. Doukas, T. R. Huang, and W. Naylor, *A New Approach to Black Hole Quasinormal Modes: A Review of the Asymptotic Iteration Method*, Adv. Math. Phys. **2012** (2012) 281705, [[arXiv:1111.5024](#)].
- [93] G. T. Horowitz and V. E. Hubeny, *Quasinormal modes of AdS black holes and the approach to thermal equilibrium*, Phys. Rev. D **62** (2000) 024027, [[hep-th/9909056](#)].
- [94] E. W. Leaver, *An Analytic representation for the quasi normal modes of Kerr black holes*, Proc. Roy. Soc. Lond. A **402** (1985) 285–298.
- [95] J. P. Boyd, Chebyshev and Fourier spectral methods. Courier Corporation, 2001.
- [96] A. Jansen, *Overdamped modes in Schwarzschild-de Sitter and a Mathematica package for the numerical computation of quasinormal modes*, Eur. Phys. J. Plus **132** (2017), no. 12 546, [[arXiv:1709.09178](#)].
- [97] J.-P. Wu and P. Liu, *Quasi-normal modes of holographic system with Weyl correction and momentum dissipation*, Phys. Lett. B **780** (2018) 616–621, [[arXiv:1804.10897](#)].
- [98] G. Fu and J.-P. Wu, *EM Duality and Quasinormal Modes from Higher Derivatives with Homogeneous Disorder*, Adv. High Energy Phys. **2019** (2019) 5472310, [[arXiv:1812.11522](#)].
- [99] P. Liu, C. Niu, and C.-Y. Zhang, *Linear instability of charged massless scalar perturbation in regularized 4D charged Einstein-Gauss-Bonnet anti de-Sitter black holes*, Chin. Phys. C **45** (2021), no. 2 025111.
- [100] K. Destounis, R. P. Macedo, E. Berti, V. Cardoso, and J. L. Jaramillo, *Pseudospectrum of Reissner-Nordström black holes: Quasinormal mode instability and universality*, Phys. Rev. D **104** (2021), no. 8 084091, [[arXiv:2107.09673](#)].
- [101] J. L. Jaramillo, R. Panosso Macedo, and L. A. Sheikh, *Gravitational wave signatures of black hole quasi-normal mode instability*, [arXiv:2105.03451](#).
- [102] W. Xiong, P. Liu, C.-Y. Zhang, and C. Niu, *Quasi-normal modes of the Einstein-Maxwell-aether Black Hole*, [arXiv:2112.12523](#).
- [103] E. Berti and K. D. Kokkotas, *Asymptotic quasinormal modes of Reissner-Nordstrom and Kerr black holes*, Phys. Rev. D **68** (2003) 044027, [[hep-th/0303029](#)].
- [104] J. Jing and Q. Pan, *Quasinormal modes and second order thermodynamic phase transition*

- for Reissner-Nordstrom black hole, Phys. Lett. B **660** (2008) 13–18, [[arXiv:0802.0043](#)].
- [105] A. Ohashi and M.-a. Sakagami, *Massive quasi-normal mode*, Class. Quant. Grav. **21** (2004) 3973–3984, [[gr-qc/0407009](#)].
 - [106] R. A. Konoplya and A. V. Zhidenko, *Decay of massive scalar field in a Schwarzschild background*, Phys. Lett. B **609** (2005) 377–384, [[gr-qc/0411059](#)].
 - [107] R. A. Konoplya and A. Zhidenko, *Stability and quasinormal modes of the massive scalar field around Kerr black holes*, Phys. Rev. D **73** (2006) 124040, [[gr-qc/0605013](#)].
 - [108] A. F. Zinhailo, *Exploring unique quasinormal modes of a massive scalar field in brane-world scenarios*, Phys. Lett. B **853** (2024) 138682, [[arXiv:2403.06867](#)].
 - [109] R. A. Konoplya, *Massive vector field perturbations in the Schwarzschild background: Stability and unusual quasinormal spectrum*, Phys. Rev. D **73** (2006) 024009, [[gr-qc/0509026](#)].
 - [110] R. A. Konoplya and A. Zhidenko, *Quasinormal modes of massive fermions in Kerr spacetime: Long-lived modes and the fine structure*, Phys. Rev. D **97** (2018), no. 8 084034, [[arXiv:1712.06667](#)].
 - [111] R. A. Konoplya, A. Zhidenko, and A. F. Zinhailo, *Higher order WKB formula for quasinormal modes and grey-body factors: recipes for quick and accurate calculations*, Class. Quant. Grav. **36** (2019) 155002, [[arXiv:1904.10333](#)].